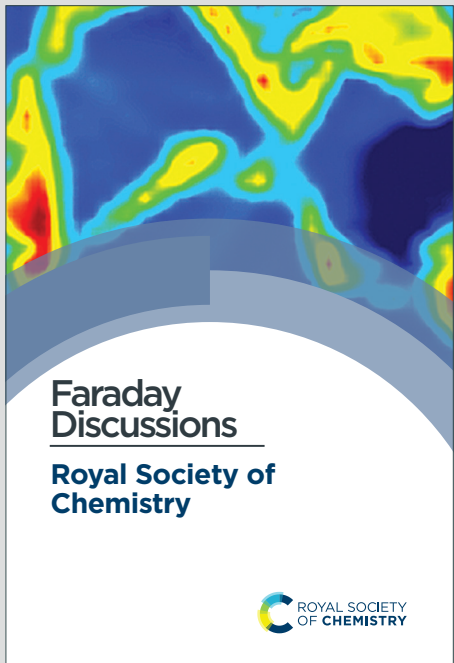


Faraday Discussions

Accepted Manuscript



This is an Accepted Manuscript, which has been through the Royal Society of Chemistry peer review process and has been accepted for publication.

Accepted Manuscripts are published online shortly after acceptance, before technical editing, formatting and proof reading. Using this free service, authors can make their results available to the community, in citable form, before we publish the edited article. We will replace this Accepted Manuscript with the edited and formatted Advance Article as soon as it is available.

You can find more information about Accepted Manuscripts in the [Information for Authors](#).

Please note that technical editing may introduce minor changes to the text and/or graphics, which may alter content. The journal's standard [Terms & Conditions](#) and the [Ethical guidelines](#) still apply. In no event shall the Royal Society of Chemistry be held responsible for any errors or omissions in this Accepted Manuscript or any consequences arising from the use of any information it contains.

This article can be cited before page numbers have been issued, to do this please use: N. Mohandas, T. N. Narayanan and A. Cuesta, *Faraday Discuss.*, 2026, DOI: 10.1039/D5FD00113G.

Structure of Interfacial Water at Gold Electrodes during Hydrogen Evolution in Alkaline Medium: A Spectroscopic Study through Isotopic Dilution

Nandita Mohandas,^a Tharangattu N. Narayanan,^a Angel Cuesta^{b,c,*}

^aTata Institute of Fundamental Research-Hyderabad, Hyderabad 500046, India.

^bAdvanced Centre for Energy and Sustainability (ACES), School of Natural and Computing Sciences, University of Aberdeen, AB24 3UE Aberdeen, Scotland, UK.

^cInstituto de Química Física Blas Cabrera, CSIC, C. Serrano 119, E-28006 Madrid, Spain.

Abstract

Driven by the persisting poor understanding of the electrocatalytic hydrogen evolution reaction (HER) in alkaline medium, we studied the interfacial water structure at a polycrystalline Au surface using *in situ* surface enhanced infrared and Raman spectroscopies. Employing an isotopic dilution strategy, we investigated the fundamental O-H and O-D vibrations of HOD molecules, where the study of the normal vibrational modes of water is simplified due to symmetry reduction. From the water structure analyses at the electrode–electrolyte interface, we unravelled the complementarities of infrared and Raman spectroscopies in probing an electrochemical interface. The major conclusions from our study are the following: (i) Interfacial water orients in a H-down manner immediately negative of the potential of zero charge (pzc); (ii) There is no strongly hydrogen-bonded ‘ice-like water’ or poorly hydrogen-bonded ‘free water’ at the Au electrode surface at any potentials. (iii) Interfacial water forms a stable backbone of water roughly parallel to the electrode surface, which survives orientation with one H down at potentials negative to pzc [Chem Sci, 2024, 15, 17469–17480], and a very high negative surface charge density is required for further reorientation. Although experiments



with H₂O suggest that the maximum degree of orientation, and therefore dielectric saturation, is reached around -0.3 V vs. RHE in 1 M KOH, the analysis of the potential dependence of the O-H and O-D stretching modes of HOD reveals that in fact, further orientation of the water dipoles continues at least down to -0.9 V.

[View Article Online](#)

DOI: 10.1039/D5FD00113G

Keywords: Isotopic Dilution; Interfacial Water Structure; Alkaline Water Electrolysis; Infrared Spectroscopy; Surface Enhanced Raman Spectroscopy.

1. Introduction

Water at interfaces plays a seminal role in processes cut across different branches of science. Water-metal interfaces are important in electrochemical energy conversion and storage systems, where the orientation and bonding of interfacial water molecules have significant impact on various electrochemical reactions. Recent studies have shown the significant role of interfacial water structure in heterogeneous electron transfer reactions.^{1–3,4–7} Many studies have tried to understand and establish a correlation between the interfacial water structure and the activity for the hydrogen evolution reaction (HER), especially in neutral and alkaline medium, due to the limited understanding of the sluggish kinetics with increase in pH.^{2,8,9} It has been suggested, using different *in situ* vibrational spectroscopy techniques, that the interfacial microenvironment, especially the activity of water (i.e., the product of the activity coefficient times the concentration of water, $a_{\text{H}_2\text{O}} = \gamma_{\text{H}_2\text{O}} c_{\text{H}_2\text{O}}$, with the standard activity of water, $a_{\text{H}_2\text{O}}^0 = 1$, corresponding to that of pure water) at the interface, serves as an important descriptor of alkaline HER kinetics.^{1–3,10–14}

Vibrational studies so far have focused on interpreting and analysing majorly the O-H stretching mode (ν_{OH}) of water, typically between 3000 and 3800 cm⁻¹, in the infrared (IR) or Raman spectra of water.^{10–13} The focus on ν_{OH} is prompted by the strong correlation between



the frequency of ν_{OH} vibration and the hydrogen-bonding strength of water, where a stronger (weaker) hydrogen-bond leads to a red-shift (blue-shift) of ν_{OH} .^{15,16} Even though ν_{OH} is an excellent indicator of the overall degree of hydrogen-bonding of water, the interpretation of the ν_{OH} band as composed of contributions from discrete molecular species with a given number of hydrogen-bonds per water molecule is inconsistent with (i) the different band shapes obtained in IR and Raman, and (ii) the vanishing of the 3250 cm^{-1} peak in both the perpendicular-polarised Raman spectrum of H_2O and in the IR and Raman O-H stretching bands of HOD, as pointed out nearly 60 years ago by Falk and Ford.¹⁷ Works over the last 20 years^{17–22} have shown that the ν_{OH} band of water is better interpreted as resulting from intra- and intermolecular intra-mode coupling (i.e., coupling between the symmetric and asymmetric ν_{OH} modes either within the same – intramolecular – or between different – intermolecular – H_2O molecules), as well as intra- and intermolecular inter-mode coupling (specifically, a Fermi resonance between the symmetric ν_{OH} mode and the first overtone at $\sim 3300 \text{ cm}^{-1}$ of the bending mode of water, δ_{HOH}).

Due to the reduction in symmetry, H-O-D has two independent ν_{OH} and ν_{OD} modes approximately 1000 cm^{-1} away from each other, which slightly reduces the degree of inter- and intramolecular intramode coupling when compared with H_2O or D_2O . Furthermore, a Fermi resonance of any of them with the overtone of δ_{HOD} ($\sim 2900 \text{ cm}^{-1}$) is not possible. This results in an overall narrowing of the vibrational line shape of the ν_{OH} and ν_{OD} bands of HOD. HOD can be easily prepared by isotopic dilution of H_2O with D_2O or vice versa. Max and Chapados showed that a solution with a 1:3 $\text{H}_2\text{O}:\text{D}_2\text{O}$ ratio, will have approximately 50% HOD and 50% D_2O , with H_2O amounting to a negligible mole fraction.^{23,24} Similarly, in a mixture with a 3:1 $\text{H}_2\text{O}:\text{D}_2\text{O}$ ratio, there will have approximately 50% HOD and 50% H_2O with negligible amount of D_2O . Thus, the ν_{OH} band in the former solution, and the ν_{OD} band in the latter, can be attributed to HOD alone.



Recent work by some of us²⁵ employed such an isotopic dilution strategy to understand the interfacial water structure at the Au-perchloric acid interface using surface-enhanced IR absorption spectroscopy in the attenuated total reflection mode (ATR-SEIRAS). It was observed that in H₂O:D₂O mixtures, the interface is always enriched in H₂O, due to the slightly larger dipole moment of D₂O. It was also understood that the potential-induced reorientation of interfacial water occurs without significant disruption of the hydrogen-bond network (other than that brought about but the mere absence of water on the metal side of the interface), and that there is a stable backbone of hydrogen-bonds parallel to the electrode surface, which needs considerable negative charge density to break. Based on that novel insight, a detailed study of the interfacial water structure in H₂O:D₂O mixtures in alkaline medium at potentials especially during HER, where the orientation and rigidity of interfacial water molecules have been proposed to determine the poor HER activity, seems promising to assess.

Both IR and Raman spectroscopies are widely used to gain information about the interfacial electrolyte structure and reaction intermediates. However, few studies make use of both techniques, assuming they provide largely overlapping information. In recent years, studies have started to look into the differences of these spectroscopic techniques when probing the interface.^{26,27} Clarke *et. al.*²⁶ developed Au film electrodes suitable for both *in situ* IR and Raman spectroscopy, and Xu *et. al.*²⁷ designed and validated an instrumental set-up with dual IR and Raman spectroscopic capabilities. These studies were focused on understanding the reaction intermediates during an electrochemical reaction, or the potential-induced adsorption/desorption of molecules on the electrode surface. The applicability of combining these spectroscopic techniques to understand the double layer structure, especially the interfacial water molecules with applied bias is worth exploring.

In this study, using the isotopic dilution strategy discussed above, we probed the interfacial water structure in alkaline aqueous electrolytes employing *in situ* ATR-SEIRAS²⁸



and surface enhanced Raman scattering (SERS)²⁹. IR and Raman spectroscopies are complementary vibrational techniques that provide information about the molecular structure.

Both techniques probe vibrational transitions between the same vibrational energy levels, but they rely on different mechanisms (absorption in IR spectroscopy and inelastic scattering in Raman spectroscopy) and obey different selection rules. Au was chosen as a model electrode and 1 M KOH (pH=14) as the electrolyte. We find that the electrolyte volume probed in SERS, in spite of the surface enhancement, is much larger than in ATR-SEIRAS, thanks to the differential nature of the latter. Making use of the recently found enrichment in H over D at the Au surface²⁵ to aid the interpretation of the differences observed between ATR-SEIRAS and SERS data, we get a better picture of the interfacial water structure, thereby leading to a better understanding of the complementarities of these two spectroscopies.

2. Results and discussions

In the following sections we majorly discuss the IR and Raman spectra of HOD molecules in two different isotopically diluted systems: 1 M KOH in both 1:3 and 3:1 H₂O:D₂O mixtures. We start with an analysis of the bulk spectra of both solutions and discuss the general differences between the two vibrational spectroscopic techniques. Following which, we will discuss the interfacial IR and Raman spectra of water, without any isotopic dilution. Later we will compare the interfacial and bulk IR and Raman spectra of the isotopically diluted systems and analyse their differences. Finally, we review the potential-induced changes in the interfacial IR and Raman spectra of the isotopically diluted systems at potentials well into the hydrogen evolution region, and unravel the complementarities of both spectroscopic techniques in elucidating the structure of interfacial water.

2.1 Raman and IR Spectra of Bulk Isotopically Diluted Alkaline Water



The IR absorbance spectra of bulk 1 M KOH solutions with $\text{H}_2\text{O:D}_2\text{O}$ ratios of 1:3 and 3:1 in the spectral region corresponding to the ν_{OH} and ν_{OD} bands of HOD, with their corresponding fit to one Gaussian curve are shown in **Figures 1A and B**, respectively. The bandwidth of both ν_{OH} and ν_{OD} of HOD is considerably narrower than that of H_2O or D_2O , due to the absence of any possible inter-mode couplings.^{21,22} For ν_{OH} , the Gaussian fit yields a full width at half maximum (FWHM) of 286 cm^{-1} with the peak centre at 3390 cm^{-1} . For ν_{OD} , FWHM was 190 cm^{-1} with the peak centre at 2500 cm^{-1} . O-D stretching bands are always narrower than O-H ones due to the reduced anharmonicity of O-D bonds.^{30,31}

The full range ATR-IR spectra of bulk 1 M KOH in H_2O , 1:3 $\text{H}_2\text{O:D}_2\text{O}$ and 3:1 $\text{H}_2\text{O:D}_2\text{O}$ are shown in **Figure S1A**. In addition to ν_{OH} and ν_{OD} , the other bands in Figure S1A are identified as follows. The band at 1650 cm^{-1} corresponds to the H-O-H bending mode (δ_{HOH}), that at 1200 cm^{-1} to the D-O-D bending (δ_{DOD}), and the H-O-D bending (δ_{HOD}) appears at 1454 cm^{-1} . The δ_{DOD} at 1200 cm^{-1} overlaps with the Si-O band of silicon dioxide (always present with Si ATR prisms), and hence will be excluded from our analysis. The negligible intensity of the δ_{HOH} and δ_{DOD} bands in 1:3 and 3:1 $\text{H}_2\text{O:D}_2\text{O}$ mixtures, respectively, testifies that the concentrations of H_2O and D_2O , respectively, are insignificant in these solutions.

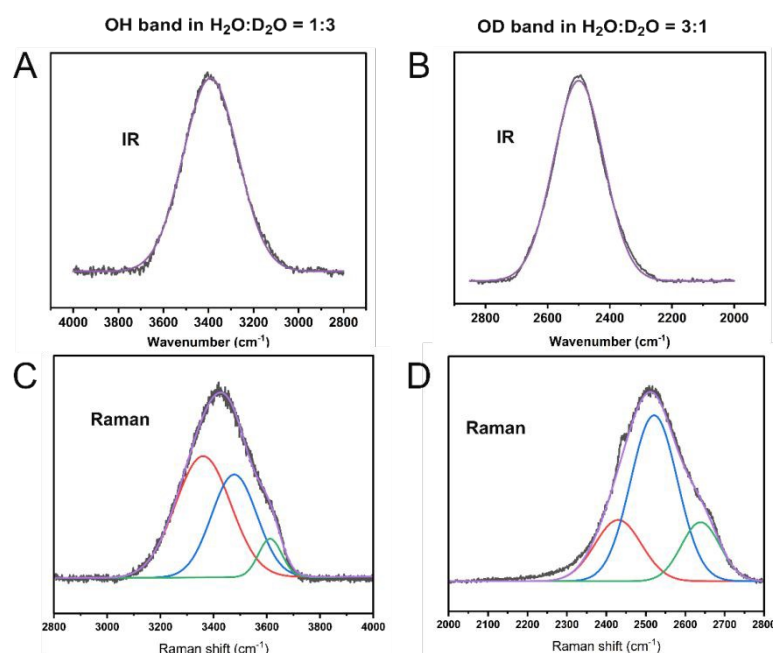


Figure 1: ATR-IR (A,B) and Raman (C,D) spectra of bulk 1 M KOH in 1:3 H₂O:D₂O (A,C) and 3:1 H₂O:D₂O (B,D) showing the O-H (A,C) and O-D (B,D) stretching bands of HOD. In A and B, the black traces correspond to the experimental ATR-IR spectra and the purple line to the corresponding Gaussian fit. The spectrum of the Si-air interface was used as background in (A) and (B). In C and D, the black traces correspond to the experimental Raman spectra and the red, blue and green lines correspond to the corresponding deconvolution into three Gaussian components. The purple trace corresponds to the sum of those three components.

Figures 1C and D show the Raman spectra of bulk 1 M KOH solutions with H₂O:D₂O ratios of 1:3 and 3:1, respectively, in the spectral region corresponding to the ν_{OH} and ν_{OD} bands of HOD. The Raman ν_{OH} and ν_{OD} bands fit well to three well-resolved Gaussian distributions. It is well known that Raman and IR vibrational spectra of water have different line shapes, which is understood as a result of the difference in their sensitivity to intermolecular coupling, where Raman is more sensitive to the coupling than IR. This is because, while in IR only dipole-dipole coupling is relevant, in Raman induced dipoles also contribute to coupling between vibrational modes.¹⁹ The ν_{OH} and ν_{OD} bands appear as strong peaks in the IR spectrum due to the strong dipole moment change, while in the Raman spectrum they may appear weaker or at different relative intensities due to the nature of the scattering process.¹⁹ Raman spectra of 1 M KOH in pure H₂O, 1:3 H₂O:D₂O, and 3:1 H₂O:D₂O in the spectral range between 1000 and 4000 cm⁻¹ are shown in **Figure S1B**. The inset in Figure S1B shows the bending mode region. As in the IR spectra, δ_{HOH} is absent in 1:3 H₂O:D₂O solution, and δ_{DOD} is absent in 3:1 H₂O:D₂O solution confirming once again that the concentrations of H₂O and D₂O, respectively, are negligible in these solutions.

Parallel-polarised Raman spectra of bulk H₂O show peaks around 3250 cm⁻¹ and 3400 cm⁻¹ and a shoulder around 3600 cm⁻¹.³²⁻³⁶ The peak at 3250 cm⁻¹ is due to a collective mode delocalised over up to 12 chromophores¹⁹ (intermolecular intra-mode coupling), and has been

shown by Sovago *et al.*³⁷ to also be affected by a Fermi resonance between the symmetric ν_{OH} of water and the overtone of the δ_{HOH} (an intramolecular inter-mode coupling). The component around 3400 cm^{-1} corresponds to a maximum in the local-mode distribution of frequencies, and the shoulder around 3600 cm^{-1} is due to hydrogen atoms not involved in hydrogen-bonds.¹⁹ The 3250 cm^{-1} peak is reduced to a shoulder in the perpendicular-polarised Raman spectrum and in the Raman ν_{OH} of HOD, both of which confirm the assignment to a coupling between modes.^{32,33}

The different IR and Raman line shapes, the vanishing of the 3250 cm^{-1} peak in both the perpendicular-polarised Raman spectrum of H_2O and in the Raman and IR ν_{OH} band of HOD are incompatible with the interpretation of the ν_{OH} band as composed of contributions from discrete molecular species with a given number of hydrogen-bonds per water molecule¹⁷ (e.g., trihedrally and tetrahedrally coordinated water). Hence, despite being highly common, such interpretations are inconsistent. Otherwise, we would obtain different distributions of specific populations of water molecules with a specific number of hydrogen-bonds from analysing, e.g., either the ν_{OH} (**Figure 1C**) or the ν_{OD} (**Figure 1D**) of HOD, which does not make sense. Nevertheless, the position of the ν_{OH} (and ν_{OD}) is still a very good reporter of the average degree of hydrogen-bonding of water.

2.2 ATR-SEIRA and SER Spectra of Interfacial Alkaline Water

We recorded interfacial IR spectra of 100% H_2O using the spectrum at 0.8 V as background (**Figure 2A**). The potential dependence of the integrated intensity of ν_{OH} is shown in **Figure S2**. The background was chosen to be 0.8 V as it is close to the pzc, as well as the onset potential for Au oxidation (please note that, in alkaline solution, the pzc of Au falls within the oxide region). Towards more negative potentials beyond 0.8 V, there is an obvious increase in the intensity of ν_{OH} and δ_{HOH} . As expected, ν_{OH} is a broad band from $3000\text{--}3700 \text{ cm}^{-1}$. Given the



broad nature of the band, and the absence of a clear main peak, any potential-induced shift of the band is difficult to identify. This contrasts with recent results by Zhu et al.¹⁴ in 0.1 M NaOH,

who identified a clear red shift of the main peak of the ν_{OH} band. The different shapes in both the cases may be attributed to the different spectral contributions of water in the solvation shells of Na^+ and K^+ . In agreement with Zhu et al.¹⁴, we see that the integrated intensity initially increases with increasingly negative potential, then levels-off around 0 V and finally remains constant below -0.4 V (The HER overpotential for Au is at ~ -0.4 V vs RHE).

The increase in the intensity can be assigned to the increased degree of orientation of interfacial water molecules with the positive end of their dipole moment pointing towards the negatively charged gold surface. The potential-induced red shift negative from the pzc can be attributed to the resulting increasingly stronger interaction of the hydrogen atoms of interfacial water with the negatively charged Au electrode.

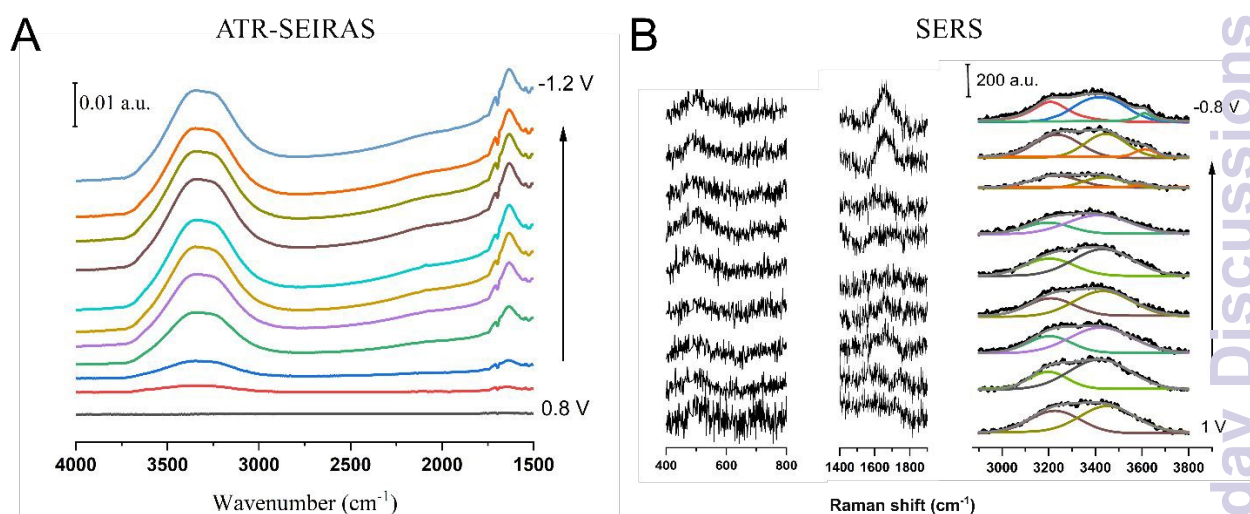


Figure 2: (A) ATR-SEIRAS and (B) SERS spectra of the Au-electrolyte interface in 1 M KOH solution (100% H₂O) within the potential regions between 0.8 and -1.2 V (A) and between 1 and -0.8 V (B). The differential spectra in (A) used the spectrum at 0.8 V as background.

We also performed SERS measurements with applied bias. The potential was varied between 1 V to -0.8 V, hence starting from the onset of oxidation to the double layer region, to finally the HER region. **Figure 2B** shows the SERS spectra of 1 M KOH (100% H₂O) as a function of the electrode potential. The ν_{OH} band of H₂O, similar to IR, is rather broad, extending from 3000 to 3700 cm⁻¹. It can be deconvoluted into two major bands, at 3200 cm⁻¹ and ~3400 cm⁻¹ down to -0.2 V, with an additional band at ~3650 cm⁻¹ emerging beyond -0.4 V. In previous work, these deconvoluted contributions have been interpreted in terms of multiple water environments: dangling OH bonds (free O-H) ~3600 cm⁻¹, OH oscillators of trihedrally coordinated hydrogen-bonded water (liquid-like water) ~3400 cm⁻¹; and tetrahedrally coordinated hydrogen-bonded water (ice-like water) ~3200 cm⁻¹.³⁸⁻⁴² As we discussed in the Introduction, this interpretation, although widely popular, is not consistent with the changes observed in the spectrum when switching from H₂O to D₂O, using isotopic mixtures, or switching from perpendicular to parallel polarisation.

In the double layer region, there were minimal changes in the water bands with potential. Only below -0.4 V there is a gradual increase in the intensity of δ_{HOH} at ~1644 cm⁻¹ and of the libration band at ~500 cm⁻¹ with increasingly negative potential, which has been attributed to interfacial water forming an ordered structure, an assignment that has been repeated in more recent work.^{2,12,13,43} An alternative assignment of the libration band at ~500 cm⁻¹ to OH⁻ was discarded⁴³ based on the absence of a band at ~3500-3700 cm⁻¹, the typical wavenumber region for the OH⁻ stretching. However, in the previous works^{2,12,13} as well as in this work, the increase in the intensity of the libration band around 500 cm⁻¹ and of δ_{HOH} at ~1644 cm⁻¹ occurs in parallel with the emergence of a band in the 3500-3700 cm⁻¹ range. Furthermore, this band in the 3500-3700 cm⁻¹ range was not observed in acidic medium (0.1 M HClO₄)² where the HER will not produce OH⁻. It is also intriguing that SERS, which shows no sensitivity to changes in



View Article Online

DOI: 10.1039/D5FD00113G

the structure of interfacial in the double-layer region, suddenly becomes surface sensitive as soon as the HER starts. For these reasons, we believe that the assignment of the bands at 3500–3700 cm^{-1} , ~1644 cm^{-1} and ~500 cm^{-1} to OH^- cannot be discarded. Further experiments to understand the origin of the libration band at ~500 cm^{-1} and OH stretching band at 3500–3700 cm^{-1} are worth exploring but are beyond the scope of this work.

2.3 Raman and IR Analysis of Isotopically Diluted Interfacial Water in Alkaline Medium

ATR-IR and Raman spectra of the bulk 1 M KOH solutions in both 1:3 and 3:1 $\text{H}_2\text{O:D}_2\text{O}$ spanning the ν_{OH} and ν_{OD} regions are shown in **Figures 3A–D**. Representative interfacial ATR-SEIRA and SER spectra are shown in **Figures 3E–H**. The expected ratio between the integrated intensity of the ν_{OH} and ν_{OD} bands (1:3 in a 1:3 mixture of $\text{H}_2\text{O:D}_2\text{O}$, 3:1 in 3:1 $\text{H}_2\text{O:D}_2\text{O}$) was obtained in both the Raman and ATR-IR spectra of the bulk solutions (**Figures 3A–D**). However, interestingly, the $\nu_{\text{OH}}:\nu_{\text{OD}}$ ratios differed between the interfacial ATR-SEIRA and SER spectra.



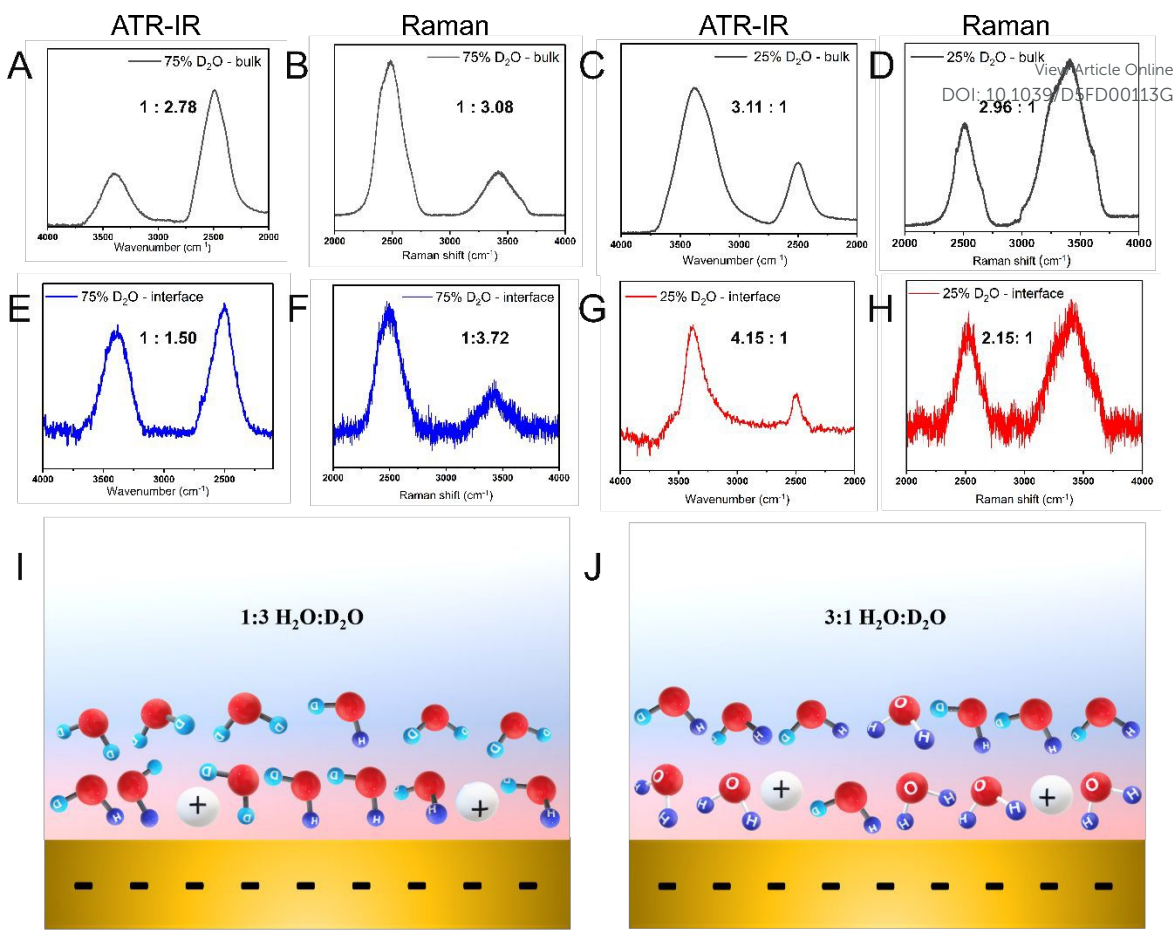


Figure 3: ATR-IR ((A) and (C)) and Raman ((B) and (D)) spectra of bulk 1 M KOH in H₂O/D₂O solutions. The spectrum of the Si-air interface was used as background in (A) and (C). Representative *in situ* ATR-SEIRA ((E) and (G)) and SER ((F) and (H)) spectra of interfacial water in the same electrolyte. A representative simplistic cartoon depicting the interfacial water populations in (I) 1:3 H₂O:D₂O and (J) 3:1 H₂O:D₂O solutions. The interfacial spectra in (E)-(H) were all recorded at 0.5 V vs. RHE. The ATR-SEIRA spectra in (E) and (G) were calculated using the spectrum at 1 V as background.

In ATR-SEIRAS, the $\nu_{\text{OH}}:\nu_{\text{OD}}$ ratio of a 1:3 mixture of H₂O:D₂O changed from 1:3 in the bulk to 1:1.5 at the interface (**Figure 3C**), and from 3:1 in the bulk to 4.15:1 at the interface in 3:1 H₂O:D₂O. In other words, ATR-SEIRAS suggests the depletion from the interface of the component of the mixture containing more deuterium. On the contrary, in SERS the $\nu_{\text{OH}}:\nu_{\text{OD}}$

ratio became 1:3.72 at the interface in 1:3 H₂O:D₂O solution (**Figure 3D**) and 2.15:1 in 3:1 in H₂O:D₂O solution. Hence, SERS suggests exactly the opposite, namely, an enrichment at the interface of the component of the mixture containing more deuterium. An increase of the intensity of the ν_{OH} band in ATR-SEIRAS has been recently reported at the Au / 0.1 M HClO₄ interface,²⁵ where it was attributed to the lower polarity of O-H bond and the slight hydrophobicity of Au. This hypothesis was supported by the clearly larger contact angle of D₂O than H₂O on a Au-coated Si prism.²⁵

To verify that the complete opposite effect (i.e., a more intense ν_{OD} band at the interface than expected from the H₂O:D₂O ratio) observed in SERS is not a consequence of the different surfaces employed for SEIRAS and SERS, we checked the contact angles of H₂O and D₂O on the Au nanoparticle (~50 nm) coated Au electrode surface used for SERS (**Figure S3**). The contact angle with H₂O was $66.0 \pm 0.3^\circ$, which increased with D₂O to $82.0 \pm 0.4^\circ$, very similar to the values reported for the Au-coated Si prism used for ATR-SEIRAS.²⁵ Hence, we can conclude that the difference in the interfacial $\nu_{\text{OH}}:\nu_{\text{OD}}$ ratios observed between the two techniques is a consequence of the differences in spectroscopic method and data collection.

In SERS, the incident laser has to penetrate the bulk electrolyte layer to reach the electrode, the whole of which contributes to the spectrum because Raman spectra are absolute, not differential. The Rayleigh range, or the effective spot area, of the laser beam in Raman spectroscopy, when calculated for the laser objective that we employed (50x Large) was found to be $\sim 3 \mu\text{m}$ (calculation details in SI). Taking into account the typical thickness of the electrolyte layer between the electrode and the electrolyte window (~1 mm) and the concentration of water in pure water (~55.6 M), a rough estimate of 10^{-9} mol of bulk water contribute to the Raman spectrum in SERS. One monolayer on Au corresponds roughly to a surface excess of 10^{-9} mol cm⁻². Within the $\sim 3 \mu\text{m}$ spot area, approximately 10^{-16} mol of interfacial water molecules will be probed by the beam. Even with the SERS effect and



assuming an enhancement factor of 10^5 , as discussed elaborately by Wang *et al.*,²⁹ the interfacial spectra will therefore have a significant contribution of bulk water. Hence the combination of the plasmonic enhancement of the Au nanoparticles and the thin water layer between the working electrode and the quartz window where the Raman laser is focused cannot completely avoid the SER spectrum being dominated by the bulk contribution, even though that minimises it.

On the contrary, ATR-SEIRAS takes advantage of the attenuated total reflection (ATR) configuration to minimise the thickness of the electrolyte layer through which the IR beam has to travel, and can cancel the still dominating contribution of interfacial water by subtraction of an adequate background (IR absorbance spectra are always differential and, by subtracting a background, only bands due to changes in the amount of IR radiation absorbed contribute to the spectrum; because the electrode potential is screened beyond the electrical double layer, bulk water will not react to a change in the applied potential, and absorbance by bulk water in the sample spectrum will be cancelled by that of bulk water in the background). Furthermore, due to damping of the evanescent wave by the metal film (the skin depth of Au in the IR frequency range 4000 cm^{-1} to 1000 cm^{-1} is $\sim 24\text{ nm}$, calculation details in SI), with typical thickness of the Au films around $\sim 10\text{-}20\text{ nm}$, only a layer of electrolyte between some nm and some tens of nm is probed, with species absorbing the more strongly the closer to the electrode surface, due to the SEIRA effect.

Hence, it is reasonable to believe that with ATR-SEIRAS we probe exclusively water within the double layer region of the electrode surface. Hence, we can conclude that there is always an H enrichment at the interface. This implies in a 3:1 $\text{H}_2\text{O:D}_2\text{O}$ solution, with only H_2O and HOD molecules (and no D_2O molecules), there will be higher proportion of H_2O at the interface than HOD. On the other hand, in a 1:3 $\text{H}_2\text{O:D}_2\text{O}$ solution, with only HOD and D_2O molecules (and no H_2O molecules), HOD molecules dominating the interface is expected.



Representative cartoons with simplified views of both these scenarios are shown in **Figure 3I and J.**

In SERS, as discussed above, the amplified signal contains information of interfacial water along with water away from the interface due to the spatial distribution of hotspots within several layers of water plus the contribution from molecules in the optical path of the excitation beam. Because the overall H:D ratio must remain 1:3 or 3:1, a hydrogen enrichment at the electrical double layer must imply a D enrichment in the layers above it. Adding the contribution of an H-enriched electrical double layer to that of the D-enriched layers adjacent to it should return a 3:1 ratio and SERS bands approaching an intensity ratio similar to that in the bulk Raman spectra, maybe with a slightly more intense-than-expected O-H band due to the larger SER effect affecting species closer to the surface. However, the SER effect also depends strongly on the wavelength-dependent magnitude of the plasmon resonance. Au spherical nanoparticles typically show a plasmon resonance maximum close to 500 nm with a decaying tail at higher frequencies. Given the smaller Raman shift of the O-D stretching, the corresponding Stokes scattered photons will be closer to the excitation wavelength (632 nm) than those corresponding to the O-H stretching, and can experience a larger SER effect.⁴⁴ Even a modest plasmonic advantage for the OD scattered wavelength could result in a non-negligible larger SER effect because the latter depends on the square of the electric field, and could compensate for the hydrogen enrichment at the interface. Hence, direct correlation between SERS intensity and quantitative composition is not as straightforward as in the case of ATR-SEIRAS, where enhancement factors are smaller and wavelengths far from the plasmon resonance maximum are used.

2.4 Potential Dependence of the ATR-SEIRA Spectra of Isotopically Diluted Interfacial Water



The potential-dependent structure of interfacial water was probed by *in-situ* ATR-SEIRAS to gain insights about the potential-induced reorientation and the hydrogen-bonding

[View Article Online](#)

DOI: 10.1039/D5FD00113G

network of water at the Au surface. The cyclic voltammogram (CV) of the Au film (**Figure S4A**) confirms that the prepared film is a neat polycrystalline Au surface. We have focused our attention on understanding the ν_{OH} band in the case of 1:3 H₂O:D₂O solution, as it arises solely from HOD molecule. Similarly, and for the same reason, in 3:1 H₂O:D₂O solution, we have analysed the ν_{OD} band.

During the *in-situ* ATR-SEIRAS spectra, the potential was first scanned from 0 to 1 V at a scan rate of 5 mV s⁻¹ (CV shown in **Figure S4B**), with an interval of 0.09 V between spectra. We will refer to this as the double layer region (dl region), although it includes the onset of surface oxidation at its positive limit. Similarly, the potential was also scanned from 0 V to -1 V (CV in **Figure S4C**), which is referred to as the HER region. **Figures 4A and B** show the *in-situ* ATR-SEIRAS spectra in the ν_{OH} region in 1:3 H₂O:D₂O, while **Figures 4C and D** show spectra in the ν_{OD} region in 3:1 H₂O:D₂O. In all the cases, although the background was recorded at 0 V, the spectra were recalculated using the spectrum at 1 V as background (i.e., closest to the pzc) for the dl region, and that at -1 V for the HER region for easy interpretation of the spectra.



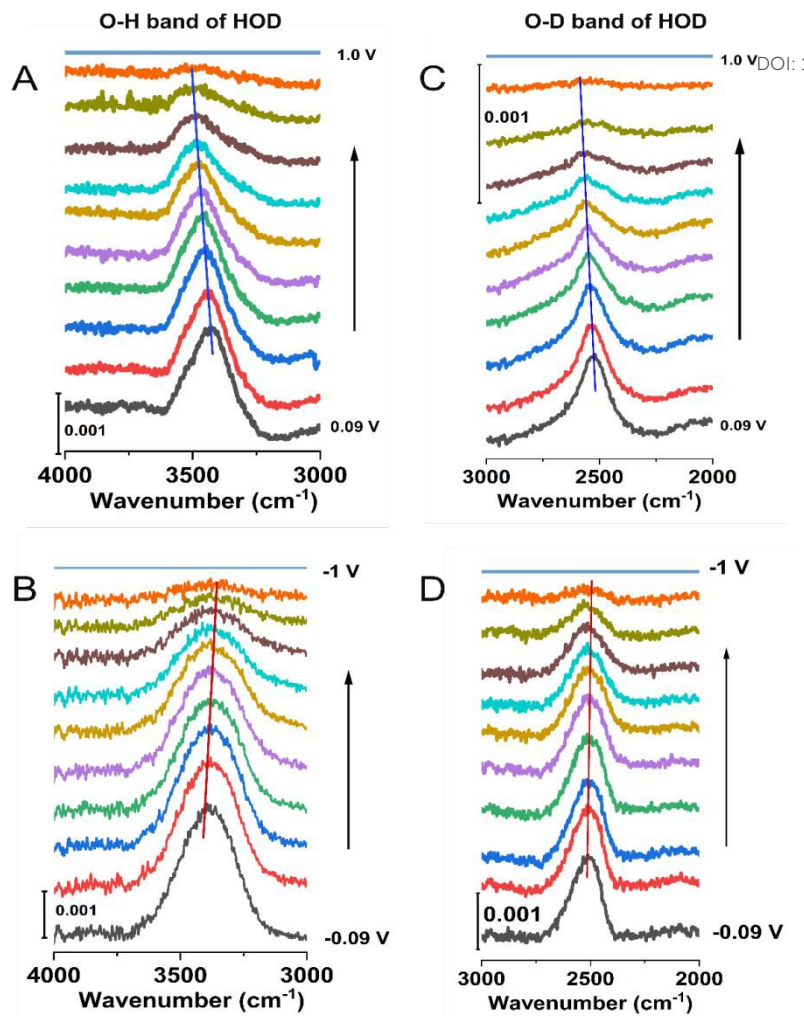


Figure 4: *In-situ* potential-dependent ATR-SEIRA spectra in the ν_{OH} (A,B) and ν_{OD} (C,D) region of HOD in the double layer (A,C) and HER (B) regions. Spectra were recorded using 0.1 M KOH solutions either in 1:3 H₂O:D₂O (A,B) or in 3:1 H₂O:D₂O (C,D). The vertical blue (A,C) and red (B,D) lines are a guide to the eye showing the trend in the potential evolution of the ν_{OH} and ν_{OD} frequencies.

As expected, other than the narrower bandwidth of ν_{OD} , the potential dependence of ν_{OH} and ν_{OD} in the spectra in **Figures 4A-D** is very similar. Furthermore, the evolution of the spectra in the dl region (**Figures 4A and C**) is consistent with recent work in acidic medium.²⁵ We observe that the ν_{OH} and ν_{OD} bands increase in intensity and red-shift as the potential is scanned away from the pzc towards less positive potentials (please note that such red-shift was not so

evident in the potential dependent spectra in 1M KOH in 100% H₂O, Figure 2A). Here again, same as the case of 100% H₂O, the increase in the intensity can be assigned to the reorientation of interfacial water molecules at the negatively charged gold surface. The red shift with increasing negative potential continues into the HER region (**Figures 4B and D**), which is consistent with the expected increase in the degree of interaction of the hydrogen atoms of water with the metal surface.

It is intriguing however that, instead of the intensity saturation observed in the ν_{OH} band in 100% H₂O (Figure S2), the intensity of the ν_{OH} and ν_{OD} bands of HOD remain roughly constant between 0 and -0.3 V and then clearly decreases with increasing negative potential. **Figures 5A and B** track the changes with potential in the integrated peak intensity and peak position of ν_{OH} and ν_{OD} . Between 0.1 and -0.5 V, the integrated intensity is nearly independent of potential (ν_{OD}) or decreases rather slowly (ν_{OH}), and starts decreasing faster beyond -0.5 V, roughly mirroring the HER current in the CV.



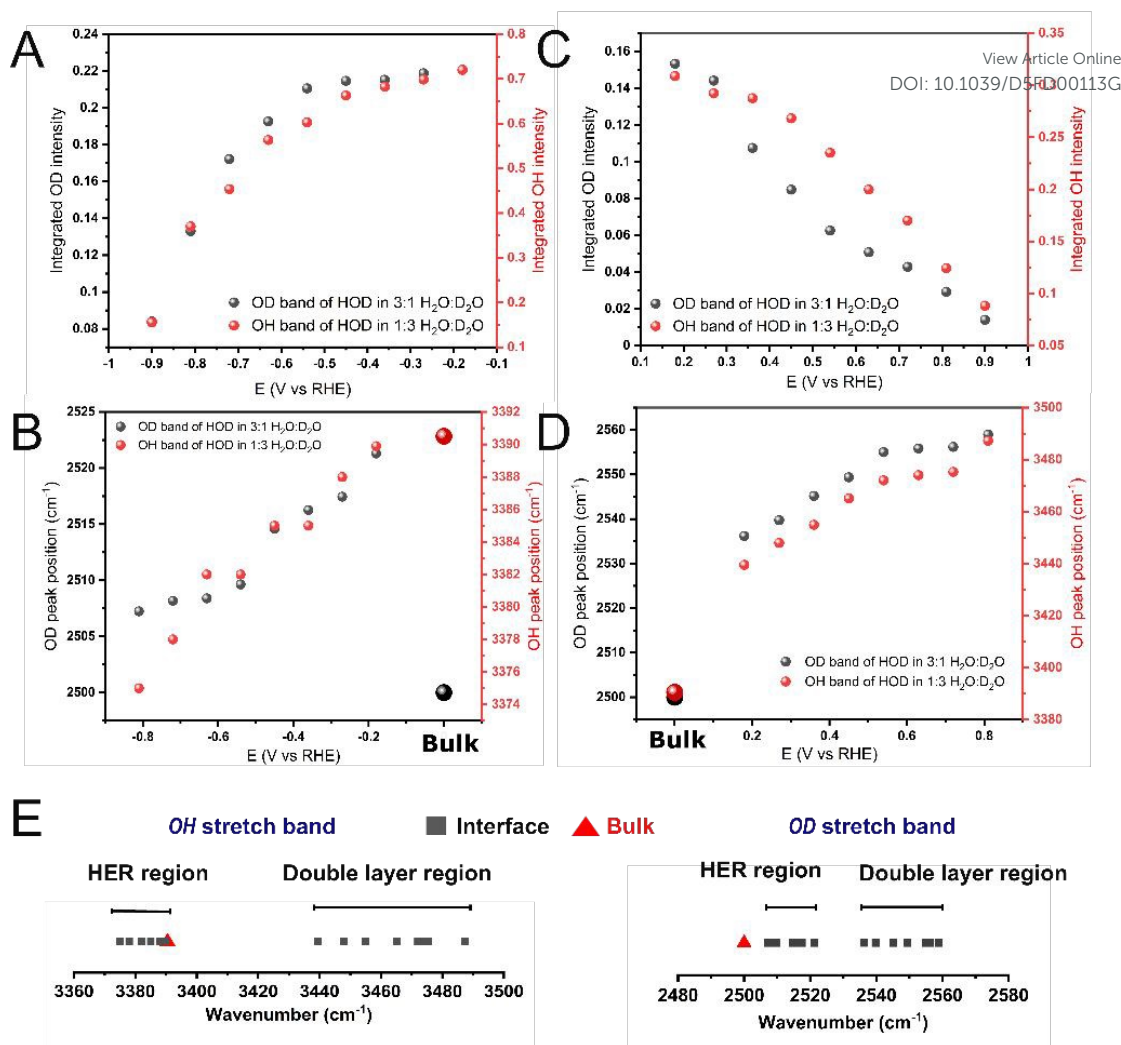


Figure 5: The change in the integrated band intensity and the peak position of in the HER region (A, B) and dl region (C,D). (E) The range of wavenumbers of the ν_{OH} and ν_{OD} bands in the dl and HER region as compared to the bulk solution.

A possible explanation for this is the following. Two O-H bonds are involved in ν_{OH} of H₂O, while only one O-H (or O-D) bond is probed in ν_{OH} (or ν_{OD}) of HOD. Hence, the angle between the relevant transition dipole moment and the normal to the surface will be different in each of these cases. We can understand the intensity maximum of ν_{OH} (or ν_{OD}) of HOD at a less negative potential than ν_{OH} of H₂O (maximum intensity of ν_{OH} and ν_{OD} of HOD is reached between 0.15 and -0.15 V, Figure 4, maximum intensity in ν_{OH} of H₂O is reached at -0.4 V, Figure 2A) as a consequence of this. As water continues to respond to the applied electric field,



the population of HOD molecules with either the O-H (or O-D) bond perpendicular to the surface will decrease. This can explain why after reaching a maximum, the intensity of ν_{OH} and ν_{OD} of HOD shows a decrement. But, unlike the direction of the transition dipole moments of ν_{OH} (or ν_{OD}) of HOD (that are in the direction of the O-H or O-D bond, respectively), that of the transition dipole moment of ν_{OH} of H_2O is not well-defined. It will be centred around the molecule's bisector, but, because the mode is the result of inter- and intramolecular coupling, there will be a distribution of transition dipole moments around that central direction. Hence, as water reorients, initially the population of H_2O with transition dipole moments perpendicular to the surface increases, but it will not increase beyond a maximum even if water continues orienting, leading to a constant intensity and apparent dielectric saturation. We conclude therefore that water dipoles continue to reorient and the population of water molecules with their dipole moments perpendicular to the surface continue to increase as the potential is scanned in the HER region, at least down to -1 V. This is contrary to what was concluded by Zhu et al.¹⁴ where, due to only looking at H_2O instead to also examining HOD, they suggested a dielectric saturation before the HER overpotentials were reached.

Figures 5C and D show the changes in the integrated peak intensity and peak position in the dl region. As we discussed previously, the potential dependence of ν_{OH} and ν_{OD} bands were similar, with the band increasing in intensity and red-shifting as the potential is scanned less positive (away from pzc). From **Figure 5E** we understand that for both ν_{OH} and ν_{OD} there is larger change in the peak position in the dl region when the potential is brought down from 1 V to 0 V. In the HER region despite the reaction and subsequent hydrogen generation, the change in the peak position is comparatively smaller than the dl region. This indicates that interfacial water ordering and bonding with the Au electrode surface occur to a larger extend at potentials immediately negative of the pzc. This is in line with what was observed in Au-perchloric acid system where water was found to be already oriented in a H-down fashion at

View Article Online

DOI: 10.1039/D5FD00113G



potentials negative of pzc.²⁵ At the same time, once a given number of molecules have one of their O-H bonds pointing towards Au, there is a barrier for further orientation with both O-H bonds pointing to the surface. Only when the barrier is overcome, the population of water molecules with both H pointing to the surface starts increasing with high negative potentials.

Another important observation from **Figure 5E** is that the ν_{OH} band in the dl region is blue-shifted, and that in the HER region is red-shifted with respect to the bulk ν_{OH} band. However, in the case of ν_{OD} , both in the HER and the dl region, the band is always blue-shifted with respect to bulk ν_{OD} . The blue shift of both ν_{OH} and ν_{OD} in the dl region with respect to their values in bulk HOD is consistent with a lower degree of hydrogen bonding in interfacial water due to the presence of the electrode surface, while the continuous red-shift of these bands with increasingly negative potential reflects the increasingly stronger interaction of the H and D atoms of HOD with gold as the O-D and O-H bonds become more perpendicular to the electrode surface. However, based on the observed enrichment of the interface in hydrogen, we would expect the interaction of H with the gold surface to be stronger than that of D, which would lead to the observed faster decrease of the O-H stretching frequency with potential, eventually leading to ν_{OH} of interfacial HOD becoming lower than that in bulk HOD, whereas that of ν_{OD} remains slightly higher.

The full range ATR-SEIRA spectra as obtained for all the potentials from 1 V to -1 V for both 1:3 and 3:1 H₂O:D₂O electrolyte solutions, respectively, are shown in **Figures S5 and S6** with background taken at 0 V. Along with ν_{OH} and ν_{OD} , δ_{HOH} and δ_{HOD} can also be observed in the spectra. **Figure 6** shows only the bending region of H₂O and HOD extracted from Figure S6 and S7. The nature of the bending bands in the dl region is in line with the ν_{OH} and ν_{OD} bands, where all the bands are aligned in the same direction. Compared to the δ_{HOD} band in the bulk at 1454 cm⁻¹, we find the δ_{HOD} band of interfacial water in the dl region to be red shifted



to 1417 cm^{-1} and 1421 cm^{-1} in 1:3 and 3:1 $\text{H}_2\text{O:D}_2\text{O}$, respectively, (Figure 6A and B), which is also consistent the changes in the ν_{OH} and ν_{OD} bands (Figure 4A and C).

[View Article Online](#)
DOI: 10.1039/D5FD00113G

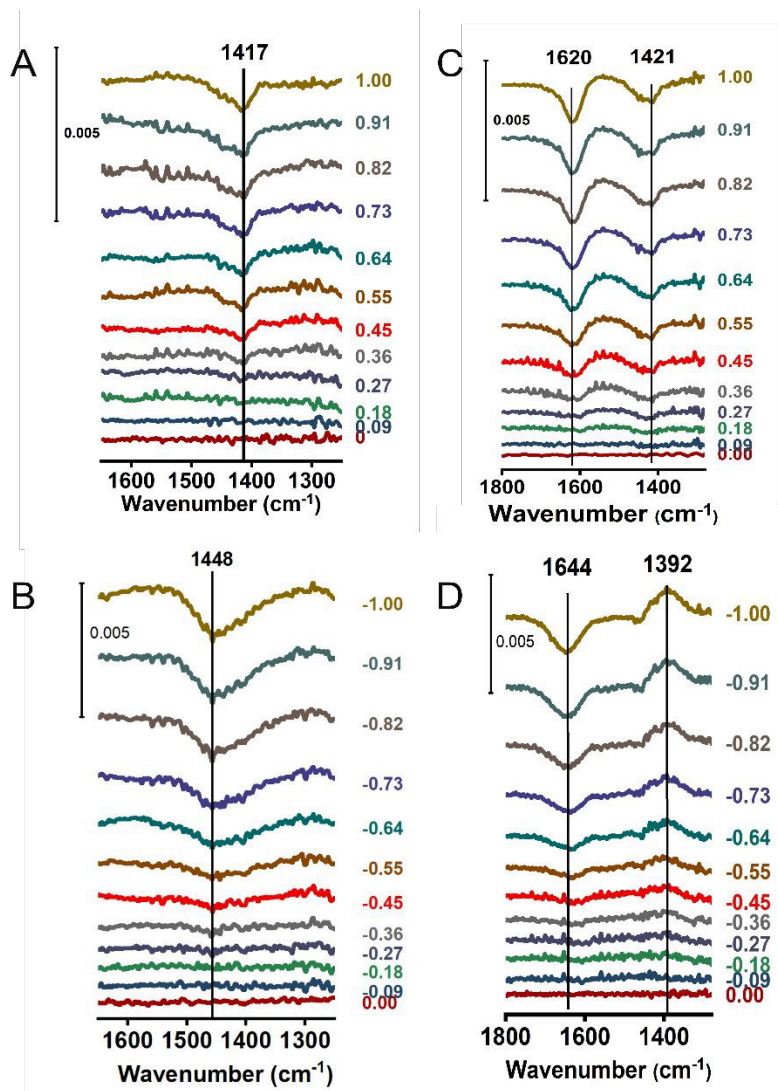


Figure 6: The bending band region of 1:3 $\text{H}_2\text{O:D}_2\text{O}$ in (A) the dl region and (B) HER region.

The bending band region of 3:1 $\text{H}_2\text{O:D}_2\text{O}$ in the (C) dl region and (D) HER region.

Although the potential dependence of the intensity of both δ_{HOH} and δ_{HOD} (δ_{DOD} overlaps with the silicon oxide band and is difficult to analyse) with potential in the dl region follows, as expected, that of ν_{OH} and ν_{OD} and can be easily explained as resulting from the reorientation of HOD in response to changes in the interfacial electric field, the potential

dependence of δ_{HOH} and δ_{HOD} in the HER region is intriguing. Based on the conclusions reached above from analysing the evolution of the intensity of ν_{OH} and ν_{OD} of HOD regarding the reorientation of interfacial water in the HER region, we would expect the intensity of δ_{HOH} and δ_{HOD} and δ_{DOD} to increase with increasingly negative potential (the transition dipole moment of these modes is parallel to the molecule's bisector). However, in 3:1 D₂O:H₂O, the intensity of δ_{HOD} decreases with increasingly negative potential (the potential dependence of δ_{DOD} can unfortunately not be properly analysed due to its overlap with the silicon oxide band at 1200 cm⁻¹), while in 1:3 D₂O:H₂O, the intensity of δ_{HOH} while that of δ_{HOD} increases. These results cannot be explained based on the reorientation of interfacial water. Instead, they might just reflect a kinetic isotope effect of the HER.

Due to the mass of D being twice that of H, we would expect breaking an O-H bond to be faster than breaking an O-D bond. Typical values for H/D primary kinetic isotope effects (i.e., when, as in this case, a bond to the isotopically labelled atom is being formed or broken) lie between 2 and 7, but can be as high as 20 (i.e., the rate of breaking an O-H bond can be as much as 20 times faster than breaking an O-D bond) or even higher at low temperatures.⁴⁵ In such a scenario, the component of the mixture with more H, (HOD in 3:1 D₂O:H₂O, H₂O in 1:3 D₂O:H₂O) will be consumed faster, resulting in the interface being depleted from HOD and enriched in D₂O in 3:1 D₂O:H₂O, as in **Figure 6C**, and being depleted from H₂O and enriched in HOD in 1:3 D₂O:H₂O, as in **Figure 6D**.

2.5 Potential Dependence of the SER Spectra of Isotopically Diluted Interfacial Water

In an attempt to add to our understanding of the interfacial water structure and its dependence on the applied potential by examining the vibrational modes of HOD, we performed *in-situ* SERS measurements with isotopically diluted solutions of 1 M KOH.

Figures 7A and B show the ν_{OH} and ν_{OD} bands of HOD in 1:3 and 3:1 H₂O:D₂O, respectively.

[View Article Online](#)

DOI: 10.1039/D5FD00113G

The ν_{OH} (**Figure 7A**) and ν_{OD} (**Figure 7B**) bands of interfacial HOD are much narrower than ν_{OH} of interfacial H₂O (Figure 2B), for the reasons already explained above, and can be fit to a single Gaussian peak at $\sim 3400 \text{ cm}^{-1}$ (ν_{OH}) and 2450 cm^{-1} (ν_{OD}).

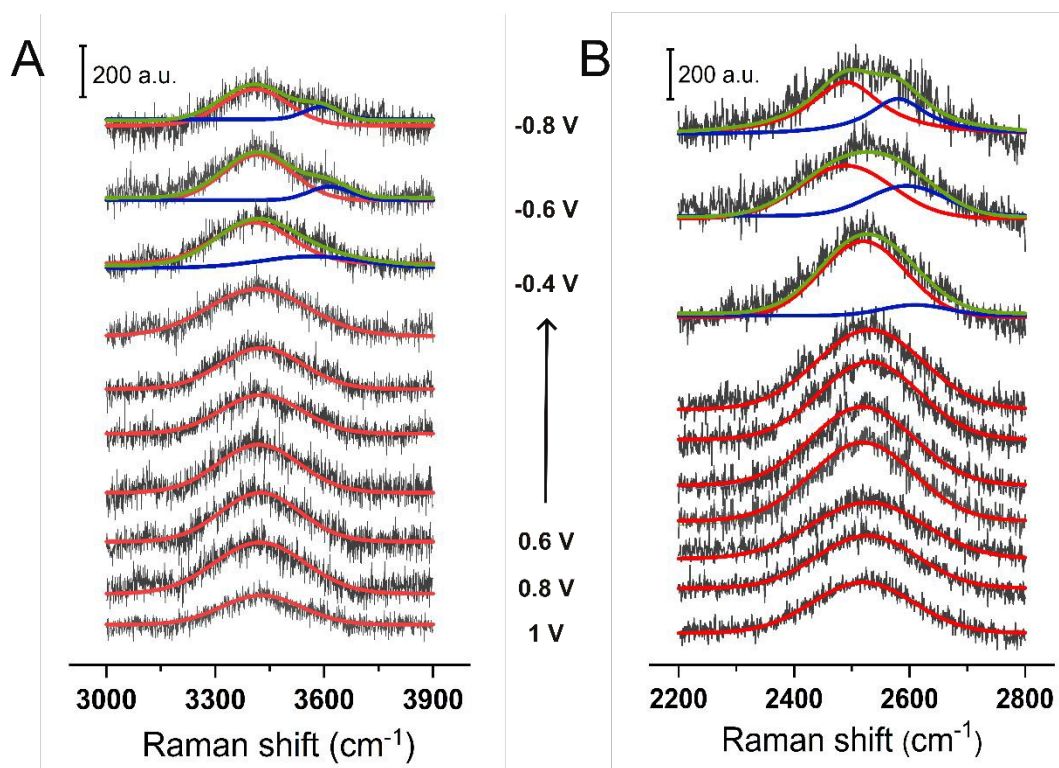


Figure 7: The changes in (A) ν_{OH} band in 1:3 H₂O:D₂O solution and (B) ν_{OD} band of H-O-D 3:1 H₂O:D₂O with applied bias.

Very little changes, if any, can be seen in the spectra as the potential is scanned negatively, except for shoulders around 3600 cm^{-1} (Figure 7A) and around 2650 cm^{-1} (Figure 7B) emerging at $E < -0.4 \text{ V}$. These high-frequency components have been assigned in the past to dangling OH bonds (free O-H) but, as discussed above, we find an assignment of these bands to either OH- produced in the HER or to weakly hydrogen-bonded water molecules in the solvation shell of K⁺¹⁴ more reasonable. In other words, SERS provides very little information regarding potential-induced changes in the structure of interfacial water. This contrasts with



the high sensitivity of ATR-SEIRAS, which we have shown to be capable of monitoring with high accuracy changes in the orientation and in the degree of hydrogen bonding of interfacial water through analysing changes in the intensity and frequency of ν_{OH} , ν_{OD} and δ_{HOD} of HOD, as well as of δ_{HOH} of H₂O in isotopic mixtures of H₂O and D₂O.

Figure S7 shows the full range potential-dependent SERS spectra for 3:1 H₂O:D₂O, where the evolution of δ_{HOH} and δ_{HOD} at 1604 and 1411 cm⁻¹, respectively, with potential, and of similar to H₂O system (Figure 2B), the libration band at 500 cm⁻¹ is observed. In the SERS spectra in 1:3 H₂O:D₂O (**Figure S8**), we observed δ_{DOD} at 1201 cm⁻¹ and δ_{HOD} at 1414 cm⁻¹. The OD libration bands were difficult to observe in our spectra, as they occur well below 200 cm⁻¹. In all cases, we only observe changes in these bands at $E < -0.4$ V, which supports our argument that they are not due to changes in the orientation and structure of interfacial water, but rather to either the production of OH⁻ or the migration of K⁺ into the electrical double layer. As these were absent in the ATR-SEIRA spectra, and are not showing any significant stark shift with potential, we understand that these molecules are located beyond the first few layers of water molecules from the Au surface.

3. Conclusions

We have used *in situ* ATR-SEIRAS and SERS with the aim of identifying their suitability and complementarity to improve our understanding of the structure of water at the electrical double layer. In doing so, we have simplified the interpretation of the O-H stretching band of water by focusing on the O-D and O-H stretching of HOD, prepared by making isotopic mixtures of H₂O and D₂O of the adequate composition. We have paid particular attention to the structure of interfacial water in alkaline medium (1 M KOH) at potentials within the hydrogen evolution region.



The first conclusion of our work is that, while ATR-SEIRAS is very sensitive to potential-induced changes in the average orientation and degree of hydrogen bonding of interfacial water, SERS is dominated by bulk water and provides only limited information, if any, about the double layer structure of the interface. Wang *et al.*²⁹ have discussed this issue in detail, and have suggested the need for a manual subtraction of the Raman spectrum at a particular potential to extract the interfacial contribution. We tried this method, and subtracted the SER spectrum at 1 V from the rest of spectra (**Figure S9**). However, the subtraction made the spectra uninterpretable due to poor signal-to-noise ratio. Raman methods are therefore not well suited to study the structure of water at the electrical double layer, with the only possible exception of tip-enhanced Raman scattering⁴⁶ which can probe exclusively the few water molecules trapped within the electrode surface and the tip of a scanning tunnelling microscope located at tunnelling distance. SERS also fails at detecting the enrichment in the component of the H₂O:D₂O isotopic mixture richer in hydrogen, due to the sensitivity of the enhancement factor to the proximity of the inelastically scattered photons to the plasmon resonance maximum.

Regarding the structure and hydrogen-bonding network of interfacial water in alkaline medium, the prime conclusions of our work in a nutshell are:

1. The population of water molecules oriented in a one H-down fashion starts increasing immediately negative to the pzc of the system.
2. There is no strongly hydrogen-bonded ‘ice-like water’ or poorly hydrogen-bonded ‘free water’ at the interface in alkaline media at any potentials. In general, water at the interface is more weakly hydrogen-bonded than in the bulk.
3. Interfacial water forms a stable hydrogen-bond backbone roughly parallel to the electrode surface that survives orientation with one H down,²⁵ but needs to be broken when water orients with both H down. There is a barrier to breaking that



hydrogen backbone, which only happens at potentials well into the hydrogen evolution region in alkaline medium (between approximately -0.2 and -0.4 V vs. RHE) and very negative (between approximately -1.02 and -1.22 V) in the SHE scale. After this potential, the population of water molecules with both hydrogen atoms pointing towards the surface starts increasing with increasingly negative potential, an effect which can only be seen in the potential-dependent spectra of HOD, but not in those of H₂O or D₂O. For this reason, Zhu et al.¹⁴ concluded that dielectric saturation of water occurs around 0.15 V vs. RHE in alkaline medium (ca. -0.62 V vs. SHE), whereas our work by looking into HOD instead of H₂O shows that this must happen more negative than -1.73 V vs. SHE).

Zhu et al.¹⁴ have provided evidence that, at least on Au, the slower kinetics of the HER in alkaline media is not due to the consequence of a disruption of the hydrogen-bond network connectivity or to slower dynamics of water reorganization within the electrical double layer. Instead, they have proposed that it is due to a smaller electrochemical driving force because of the low electric potential at the reaction plane. Our results are in general consistent with this conclusion. It is true that, at pH 14, we do observe that a significant increase in the population of water molecules with both H atoms pointing towards the surface starts occurring around the potential at which the onset of the HER should be seen if the kinetics were as fast as in acidic medium. It might be argued based on this that the resulting disruption of the hydrogen-bond backbone parallel to the electrode surface is connected with the slower kinetics in alkaline medium. However, this would not be the case at lower alkaline pHs (pH < 13), at which this effect would occur at more negative potentials in the RHE scale but slower HER kinetics are still observed.



4. Experimental methods

Figure S10 shows the schematic cell set-up of the spectro-electrochemical cell used for *in situ* ATR-SEIRAS; and the flow cell set-up used for *in situ* SERS experiments. Both are home-made set-ups optimised in our labs. Photos of both the IR and Raman experimental set-ups are shown in **Figure S11**. The detailed procedures for conducting ATR-SEIRAS and SERS are explained below.

Since surface enhanced spectroscopic techniques are extremely sensitive, even minor amounts of contamination in the sample can have a large impact on the quality and interpretation of the spectroscopic data. In ATR-SEIRAS, freshly prepared Au films on well-polished Si prisms were used, which minimised the influence of impurities. Contamination from carbon impurities were a major concern in SERS even with freshly prepared Au nanoparticles deposited on a flame cleaned Au electrode. Following the protocol described in detail by Hartman *et. al.*,⁴⁷ where the substrate is cleaned with heat and oxidation treatments, we obtained featureless impurity-free SERS spectra. The effects of Raman laser power and exposure time were also optimised to ensure the changes in the water bands were laser intensity independent.

4.1 Absorbance IR spectroscopy (ATR-IR)

Absorbance IR spectra of the bulk of 0.1 M KOH solutions were recorded by using as background the spectrum collected by totally reflecting the IR beam at the Si-air interface. The surface of the same Si prism was then fully covered by a drop of the 1 M KOH solution and then the sample spectrum was recorded.

4.2 ATR-SEIRA spectroscopy



ATR-SEIRA spectra were collected with a Nicolet iS50R FTIR spectrometer equipped with an MCT detector (liquid N₂ cooled) and a home-made ATR accessory, using unpolarized light.

Each spectrum, including the background spectrum, consisting of 120 interferograms with a spectral resolution of 4 cm⁻¹ were recorded during the positive cycle of a cyclic voltammogram at a scan rate of 5 mV s⁻¹. Experiments were conducted at room temperature, approximately 22 °C, and normal atmospheric pressure. Time taken to acquire an individual spectrum at a resolution of 4 cm⁻¹ was 17.3 s. Spectra were calculated in absorbance units as $A = -\log(R_{\text{sample}} / R_{\text{background}})$, where $R_{\text{background}}$ and R_{sample} are the reference and sample spectra, respectively. The working electrode was a gold film deposited on the totally reflecting plane of a Si prism bevelled at 60°, and it was attached to the spectro-electrochemical cell using an O-ring seal. The gold layer was coated on the Si prism following an electroless deposition method.⁴⁸ An EmStat3 Potentiostat from PalmSens was used to control the potential of our working electrode during the ATR-SEIRAS experiments. Before any IR measurements, the film was cycled in the corresponding electrolyte to check its stability, clean the surface, and obtain a reproducible surface morphology. A gold mesh was used as a counter electrode and a leak-proof Ag/AgCl (KCl sat) electrode was used as a reference electrode. All of the potentials in the report are referred to the RHE scale.

4.3 SERS spectroscopy

Gold nanoparticles, synthesised using a previously reported method,^{49,50} (The UV data and SEM image are shown in **Figure S12**) was diluted and drop-casted on *polycrystalline* Au electrode surface before electrochemical SERS experiments. The gold particle drop-casted Au electrode was dried and cleaned to ensure the electrode surface is impurity free.⁴⁷ *In situ* SERS were taken using a micro-Raman spectrometer (Renishaw Invia Spectrometer) with 633 nm laser excitation using L50x lens using a homemade electrochemical cell. All the Raman spectra were recorded in reflection mode using an edge filter where only Stokes lines can be observed.



The time for recording data was optimized to 5 s with 10% laser intensity for a better signal-to-noise ratio and minimal destruction. An EmStat3 Potentiostat from PalmSens was used to control the potential of our working electrode. A graphite rod was used as a counter electrode, and a leakproof Ag/AgCl (KCl_{sat}) as the reference electrode.

[View Article Online](#)

DOI: 10.1039/D5FD00113G

Author contribution

AC conceived the idea of isotopic dilution strategy. NM, TNN and AC conceptualised the project. NM designed and performed all the experiments, with AC supervising the IR experiments and TNN supervising the Raman experiments. All authors participated in data analysis and the manuscript was written by NM with contributions from all authors.

Acknowledgements

NM and TNN acknowledge the support of the Department of Atomic Energy, Government of India, under Project Identification No. RTI 4007. NM and TNN also thank Prof. Harish N.S. Krishnamoorthy for useful discussions, Ms. Anagandula Shravani for SEM analysis, and Ms. Anusha P.P. for graphical support. AC acknowledges the support of The Leverhulme Trust through project grant RPG-2021-342.

References

1. I. Ledezma-Yanez, W. D. Z. Wallace, P. Sebastián-Pascual, V. Climent, J. M. Feliu and M. T. M. Koper, *Nat Energy*, 2017, **2**, 17031.
2. L. fan Shen, B. an Lu, Y. yang Li, J. Liu, Z. chao Huang-fu, H. Peng, J. yu Ye, X. ming Qu, J. ming Zhang, G. Li, W. bin Cai, Y. xia Jiang and S. gang Sun, *Angew Chem Int Edt*, 2020, **59**, 22397–22402.
3. X. Chen, X. T. Wang, J. B. Le, S. M. Li, X. Wang, Y. J. Zhang, P. Radjenovic, Y. Zhao, Y. H. Wang, X. M. Lin, J. C. Dong and J. F. Li, *Nat Commun*, 2023, **14**, 5289.



4 W. Ge, L. Dong, C. Wang, Y. Zhu, Z. Liu, H. Jiang and C. Li, *ACS Catal*, 2024, **14**, 10529–10537.

View Article Online
DOI: 10.1039/D5FD00113G

5 Y. Wang, J. Zhang, J. Zhao, Y. Wei, S. Chen, H. Zhao, Y. Su, S. Ding and C. Xiao, *ACS Catal*, 2024, **14**, 3457–3465.

6 Z.-Q. Zhang, S. Banerjee, V. S. Thoi and A. Shoji Hall, *J Phys Chem Lett*, 2020, **11**, 5457–5463.

7 N. Mohandas, T. N. Narayanan and A. Cuesta, *ACS Catal*, 2023, **13**, 8384–8393.

8 C. Hu, L. Zhang and J. Gong, *Energy Environ Sci*, 2019, **12**, 2620–2645.

9 R. Subbaraman, D. Tripkovic, D. Strmcnik, K.-C. Chang, M. Uchimura, A. P. Paulikas, V. Stamenkovic and N. M. Markovic, *Science*, 2011, **334**, 1256–1260.

10 P. Li, Y. Jiang, Y. Hu, Y. Men, Y. Liu, W. Cai and S. Chen, *Nat Catal*, 2022, **5**, 900–911.

11 K. Sun, X. Wu, Z. Zhuang, L. Liu, J. Fang, L. Zeng, J. Ma, S. Liu, J. Li, R. Dai, X. Tan, K. Yu, D. Liu, W. C. Cheong, A. Huang, Y. Liu, Y. Pan, H. Xiao and C. Chen, *Nat Commun*, 2022, **13**, 6260.

12 Y. H. Wang, S. Zheng, W. M. Yang, R. Y. Zhou, Q. F. He, P. Radjenovic, J. C. Dong, S. Li, J. Zheng, Z. L. Yang, G. Attard, F. Pan, Z. Q. Tian and J. F. Li, *Nature*, 2021, **600**, 81–85.

13 C. Y. Li, J. B. Le, Y. H. Wang, S. Chen, Z. L. Yang, J. F. Li, J. Cheng and Z. Q. Tian, *Nat. Mater.*, 2019, **18**, 697–701.

14 B.-Q. Zhu, E.-F. Zhen, B.-Y. Liu, L.-D. Zhang, C.-Y. Zhang, Z.-F. Liu and Y.-X. Chen, *J Catal*, 2025, **445**, 116021.

15 D. Ojha, K. Karhan and T. D. Kühne, *Sci Rep*, 2018, **8**, 16888.

16 R. Rey, K. B. Møller and J. T. Hynes, *J Phys Chem A*, 2002, **106**, 11993–11996.



17 M. Falk and T. A. Ford, *Can J Chem*, 1966, **44**, 1699–1707.

18 A. A. Kananenka and J. L. Skinner, *J Chem Phys*, 2018, **148**, 244107.

19 B. M. Auer and J. L. Skinner, *J Chem Phys*, 2018, **128**, 224511.

20 T. Seki, K. Y. Chiang, C. C. Yu, X. Yu, M. Okuno, J. Hunger, Y. Nagata and M. Bonn *J. Phys. Chem. Lett.* 2020, **11**, 19, 8459–8469.

21 M. Sovago, R. K. Campen, G. W. H. Wurpel, M. Müller, H. J. Bakker and M. Bonn, *Phys Rev Lett*, 2008, **100**, 173901.

22 J. Schaefer, E. H. G. Backus, Y. Nagata and M. Bonn, *J Phys Chem Lett*, 2016, **7**, 4591–4595.

23 J. J. Max and C. Chapados, *J Chem Phys*, 2002, **116**, 4626–4642.

24 J.-J. Max and C. Chapados, *J Chem Phys*, 2011, **134**, 164502.

25 P. Gunasekaran, X. Du, A. Burley, J. Le, J. Cheng and A. Cuesta, *Chem Sci*, 2024, **15**, 17469–17480.

26 X. Chang, S. Vijay, Y. Zhao, N. J. Oliveira, K. Chan and B. Xu, *Nat Commun*, 2022, **13**, 2656.

27 X. Xu, W.-Y. Zhang, X.-Y. Ma, X. Qin, T.-W. Jiang, H. Li, Y. Zhang, K. Jiang and W.-B. Cai, *Anal Chem*, 2025, **97**, 1047–1053.

28 A. Cuesta, *Elsevier B.V.*, 2022, **35**:101041.

29 Y.-H. Wang, S. Li, R.-Y. Zhou, S. Zheng, Y.-J. Zhang, J.-C. Dong, Z.-L. Yang, F. Pan, Z.-Q. Tian and J.-F. Li, *Nat Protoc*, 2023, **18**, 883–901.

30 J. B. Asbury, T. Steinel, K. Kwak, S. A. Corcelli, C. P. Lawrence, J. L. Skinner and M. D. Fayer, *J Chem Phys*, 2004, **121**, 12431–12446.

View Article Online
DOI: 10.1039/D5FD00113G



31 H.-K. Nienhuys, S. Woutersen, R. A. van Santen and H. J. Bakker, *J Chem Phys*, 1999, **111**, 1494–1500.

[View Article Online](#)
DOI: 10.1039/D5FD00113G

32 W. F. Murphy and H. J. Bernstein, *J Phys Chem*, 1972, **76**, 1147–1152.

33 J. R. Scherer, M. K. Go and S. Kint, *J Phys Chem*, 1974, **78**, 1304–1313.

34 G. E. Walrafen, M. S. Hokmabadi and W.-H. Yang, *J Chem Phys*, 1986, **85**, 6964–6969.

35 D. M. Carey and G. M. Korenowski, *J Chem Phys*, 1998, **108**, 2669–2675.

36 D. E. Hare and C. M. Sorensen, *J Chem Phys*, 1992, **96**, 13–22.

37 M. Sovago, R. K. Campen, G. W. H. Wurpel, M. Müller, H. J. Bakker and M. Bonn, *Phys Rev Lett*, 2008, **100**, 173901.

38 Y. R. Shen and V. Ostroverkhov, *Chem Rev*, 2006, **106**, 1140–1154.

39 W. Zheng and A. Tadjeeddine, *J Chem Phys*, 2003, **119**, 13096–13099.

40 K. Ataka, T. Yotsuyanagi and M. Osawa, *J Phys Chem*, 1996, **100**, 10664–10672.

41 K. Ataka and M. Osawa, *Langmuir*, 1998, **14**, 951–959.

42 Z.-Q. Tian, B. Ren, Y.-X. Chen, S.-Z. Zou and B.-W. Mao, *Faraday Transactions*, 1996, **92**, 3829.

43 Y. X. Chen, S. Z. Zou, K. Q. Huang and Z. Q. Tian, *J Raman Spectro*, 1998, **29**, 749–756.

44 Y. Chu, M.G. Banaee and K.B. Crozier *ACS Nano* 2010, **4**, 5, 2804–2810.

45 H. Kwart, *Acc Chem Res*, 1982, **15**, 401–408.

46 J. H. K. Pfisterer and K. F. Domke. *Current Opinion in Electrochemistry* 2018, **8**, 96–102.

47 T. Hartman, C. S. Wondergem and B. M. Weckhuysen, *ChemPhysChem*, 2018, **19**, 2461–2467.



48 O. Ayemoba and A. Cuesta, *ACS Appl Mater Interfaces*, 2017, **9**, 27377–27382.

[View Article Online](#)

DOI: 10.1039/D5FD00113G

49 H. Fathima, N. Mohandas, B. S. Varghese, P. Anupkumar, R. S. Swathi and K. G. Thomas,

The J Phys Chem C, 2021, **125**, 16024–16032.

50 N. G. Bastús, J. Comenge and V. Puntes, *Langmuir*, 2011, **27**, 11098–1110.



Data Availability Statement

[View Article Online](#)

DOI: 10.1039/D5FD00113G

Data for this article are available at ScienceDB <https://doi.org/10.57760/sciencedb.31110>.